Origin of colossal permittivity in $BaTiO_3$ via broadband dielectric spectroscopy

Hyuksu Han,[1,a)] Christophe Voisin,[2] Sophie Guillemet-Fritsch,[2] Pascal Dufour,[2] Christophe Tenailleau,[2] Christopher Turner,[1] and Juan C. Nino[1]
[1]*Department of Materials Science and Engineering University of Florida, Gainesville, Florida 32611, USA*
[2]*CNRS, Institut Carnot CIRIMAT, UMR CNRS-UPS-INP 5085, Université Paul-Sabatier, 118 route de Narbonne, 31062 Toulouse Cedex 9, France*

Barium titanate (BT) ceramics with Ba/Ti ratios of 0.95 and 1.00 were synthesized using spark plasma sintering (SPS) technique. Dielectric spectroscopy (frequency range from 40 Hz to 1 MHz and temperature range from 300 K to 30 K) was performed on those ceramics (SPS BT). SPS BT showed extremely high permittivity up to $\sim 10^5$, which can be referred to as colossal permittivity, with relatively low dielectric loss of $\sim$0.05. Data analyses following Debye relaxation and universal dielectric response models indicate that the origin of colossal permittivity in BT ceramics is the result of a hopping polaron within semiconducting grains in combination with interfacial polarization at the insulating grain boundary. Furthermore, the contributions of each polarization mechanism to the colossal permittivity in SPS BT, such as a hopping polarization, internal barrier layer capacitance effect, and electrode effect, were estimated.

I. INTRODUCTION

Barium titanate ($BaTiO_3$, BT) is a material well-known for its excellent dielectric ($\varepsilon' \approx 3500$) and piezoelectric properties (190 pC/N), which allows for its utilization in a variety of electronic applications such as capacitors.[1,2] The high relative permittivity and low dielectric loss of the material are favored in the microelectronics industry since it enables device miniaturization. The relative permittivity of BT can be varied in the range of 4000–6000 depending on the grain size of the sintered ceramic, and the maximum relative permittivity can be typically achieved at the grain size of about 1 μm when sintered through conventional sintering methods.[3]

However, it was recently reported that abnormally high relative permittivity ($\varepsilon' \approx 10^4$–$10^5$) can be induced in the synthesized nano-crystalline (250 nm) BT ceramic using starting nano-crystalline BT powder and spark plasma sintering (SPS) technique.[4] This extremely high relative permittivity has been referred to as colossal permittivity.[4] SPS is a fast sintering technique that allows for the densification of ceramics while maintaining small grain size due to the short sintering time and relatively low sintering temperatures employed. A number of research groups have investigated and reported dielectric properties of SPS BT (spark plasma sintered barium titanate) ceramics.[4–7] High relative permittivity has also been found in a number of ceramics and composites such as $CaCu_3Ti_4O_{12}$ (CCTO), $Ba(Zr_{0.2}Ti_{0.8})O_3$-carbon nanotube, and BT-Ni particle composites.[8–10]

At first, it was originally thought that colossal permittivity might be related with a new intrinsic polarization mechanism due to crystal structure and/or electrical charge ordering. However, although there is an ongoing debate regarding the exact mechanisms and explanations for the origin of colossal permittivity in BT ceramics, a number of investigations have revealed that, in some cases, colossal permittivity can be attributed to a well-known extrinsic Maxwell-Wagner (MW) polarization associated with inhomogeneous electrical properties between grains and grain boundaries.[4,11–13]

In this work, colossal permittivity was induced by using SPS technique and nano-crystalline BT starting powder. Dielectric spectroscopy analysis was performed on SPS BT ceramics in order to better understand and investigate the polarization mechanisms associated with colossal permittivity of BT ceramic. Here, we show that in addition to interfacial polarization mechanism, which has been widely accepted for the origin of colossal permittivity in BT ceramics, a hopping polaron mechanism co-exists as an additional polarization mechanism contributing to the colossal permittivity of BT ceramics.

II. EXPERIMENTAL

A. Sintering and annealing

The starting BT powder was synthesized by an oxalate route previously described in detail elsewhere.[14] Briefly, $BaCl_2.2H_2O$ and $TiCl_3$ were used to synthesize the starting powders. SPS was performed on the synthesized powder by means of a Dr. Sinter 2080 from Sumimoto Coal Mining (SPS Syntx Inc., Dr. Sinter 2080). Approximately 0.9 g of powder without binder was placed in a 8 mm diameter graphite die and then sintered at 1150 °C with a dwell time of 3 min under 50 MPa of mechanical stress and electric current up to 350 A. A heating rate of 25 °C/min was used to reach the sintering temperature of 1150 °C from 600 °C. After 3 min dwelling, the sample was cooled down from 1150 °C

a)Author to whom correspondence should be addressed. Electronic mail: dducks82@ufl.edu.Tel.: +1 (352) 846 3793. Fax: +1 (352) 846 3355.

to 600 °C in ~1 min. A thin carbon layer was present at the surface of the as-sintered ceramic due to graphite contamination from the die. However, it was easily removed by polishing the surface of the ceramic. Due to the reducing atmosphere (vacuum) during SPS process, a post annealing treatment was performed in order to partially re-oxidize and recover the insulating characteristics of the ceramic samples. To anneal, a furnace was preheated to 850 °C and then the sample was placed into the furnace for 15 min dwell in air followed by air quenching.

B. Chemical composition, density, and microstructure

The chemical stoichiometry of the starting powder and the sintered ceramic was analyzed by inductively coupled plasma–atomic emission spectroscopy (ICP–AES, Horiba Scientific., Thermo - Optec ARL 3580). The density of the sintered ceramics was initially measured using the geometrical method and then the Archimedes method for samples showing at least 92% of the theoretical density (6.02 g/cm^3). The ceramic powder morphology and the microstructure of the sintered ceramics were investigated with a field electron gun scanning electron microscope (JEOL Ltd., 6335F FEG-SEM).

C. X-ray diffraction (XRD) and dielectric property measurements

A laboratory X-ray diffractometer equipped with a curved position sensitive detector (Inel Inc., CPS120) and a Cu X-ray tube source ($CuK_\alpha = 0.154056$ nm and $CuK_\beta = 0.154044$ nm) was used to determine the phases and crystal structure of the starting ceramic powders and the sintered ceramics. The XRD data for all the samples were measured over a period of 10 min. Prior to electrical measurements, the sintered ceramic disks were coated with thin gold electrodes (thickness ~30 nm) by sputtering (Cressington Scientific Inc., Cressington 108 Auto). The coated samples were placed in a closed cycle cryonic workstation (CTI – Cryogenics, Model 22), and dielectric properties as a function of temperature (20 K–300 K) were measured at the different frequencies (40 Hz–100 kHz) through an Agilent 4284 LCR meter. Precision impedance analyzer (Agilent Ltd., Agilent 4294A) combined with cryonic workstation was used in order to perform broadband dielectric spectroscopy analysis (40 Hz–1 MHz) in the temperature range from 20 K to 300 K.

III. RESULTS AND DISCUSSION

A. Microstructure, density, and XRD

ICP-AES results show that starting BT powders synthesized by $BaCl_2.2H_2O$ and $TiCl_3$ or $BaCl_2.2H_2O$ and $TiOCl_2$ have Ba/Ti ratios of 0.95 (BT 0.95) and 1.00 (BT 1.00), respectively. The sintered ceramics, SPS BT 0.95 and SPS BT 1.00 using BT 0.95 and 1.00 powders, were dark blue in color due to the reducing sintering atmosphere (vacuum) during SPS process.[4] The SEM images in Figure 1 shows the microstructures of freshly fractured surfaces of SPS BT 0.95 and SPS BT 1.00 ceramics with a respective average grain size of 56 ± 6 nm and 72 ± 8 nm. Grain sizes were measured

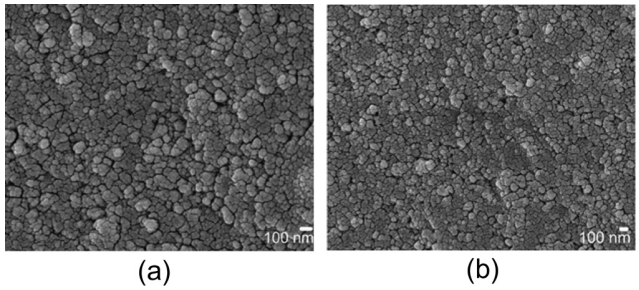

FIG. 1. SEM images for (a) SPS 0.95 and (b) SPS 1.00 sintered ceramics.

by using the mean linear intercept method of ASTM E112 standard.[15] Although the ASTM E112 method was developed for planar cross sections, it is here applied to fracture surfaces due to extremely brittle nature of SPS sintered ceramics in order to provide an estimate of the grain size of the ceramics. As expected due to the fast-firing nature of SPS technique, no significant grain growth is observed after sintering and the grain sizes of the sintered ceramics are almost in the same size as the starting powders. Density measurement by Archimedes method reveals that the both sintered ceramics have theoretical densities up to 98% (Table I).

The XRD patterns of the starting powders (BT 1.00 and BT 0.95) and the sintered ceramics (SPS BT 1.00 and SPS BT 0.95) are shown in Figure 2. No secondary phases are formed in BT 1.00 and SPS BT 1.00. However, secondary phases of $BaTi_2O_5$ (~5 vol. % relative amount) and $Ba_4Ti_{12}O_{27}$ (~7 vol. % relative amount) are observed for the Ti-rich BT 0.95 powder and SPS 0.95 ceramic, respectively. It is well known that $Ba_4Ti_{12}O_{27}$ phase is formed when Ti-rich BT powder is obtained under reduced (low P_{O2}) conditions; here the reduction of a part of Ti^{4+} to Ti^{3+} gives rise to the formation of $Ba_4Ti_2{}^{3+}Ti_{10}{}^{4+}O_{27}$.[16] Besides, both sintered ceramics of SPS BT 0.95 and 1.00 crystallized in a mixture of a cubic and a tetragonal perovskite phases which can be demonstrated by the broadening of the (200) peak. On the contrary, all of the starting powders consisted of a single cubic phase (Figure 2). This result is also well in good agreement with previous studies for SPS sintered ceramics.[17] Chemical composition, grain sizes, theoretical density, crystal lattice, and phase purity for the sintered ceramics are summarized in Table I.

B. Dielectric properties and polarization mechanisms

Relative permittivity and dielectric loss of SPS BT 0.95 and SPS BT 1.00 were measured as a function of

TABLE I. Summary of chemical composition, grain size and relative density of the sintered ceramics.

Samples	Ba/Ti ratio	Grain size (nm)	Density (%)	Structure	2nd phase
SPS BT 0.95	0.95	56 ± 6	98	C[a] + T[b]	$Ba_4Ti_{12}O_{27}$ (~7 vol. %)
SPS BT 1.00	1.00	72 ± 8	98	C + T	None

[a]C: cubic perovskite.
[b]T: tetragonal perovskite.

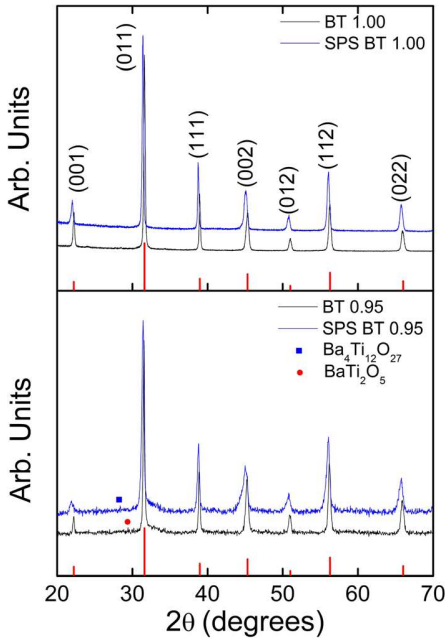

FIG. 2. The X-ray diffraction patterns for the starting powders (BT 1.00 and 0.95) and the sintered ceramics (SPS BT 1.00 and 0.95).

temperature (25 K–300 K) at different frequencies (40 Hz–100 kHz), and the results are shown in Figure 3. Extremely high permittivity of up to 10^5 with low loss ($\tan\delta \approx 0.05$) is observed at room temperature in both samples. Table II

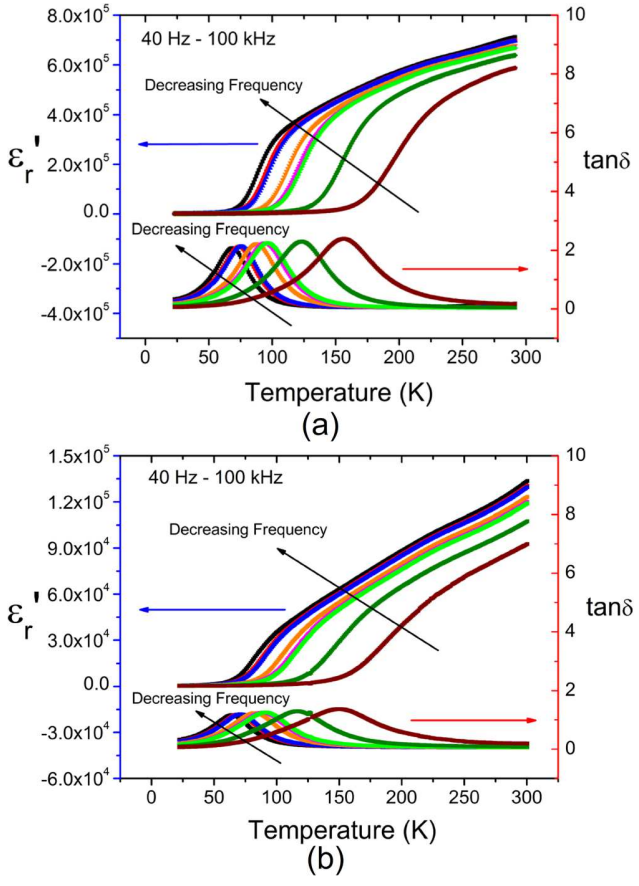

FIG. 3. Dielectric property of (a) SPS 0.95 and (b) SPS 1.00 as a function of temperature (20–300 K).

TABLE II. Dielectric property of SPS BT 0.95 and 1.00 at room temperature and 1, 10, and 100 kHz.

	1 kHz		10 kHz		100 kHz	
	ε'	$\tan\delta$	ε'	$\tan\delta$	ε'	$\tan\delta$
SPS BT 0.95	667 941	0.04	638 737	0.05	587 040	0.17
SPS BT 1.00	114 505	0.06	103 387	0.09	88 869	0.20

shows dielectric properties of SPS BT 0.95 and SPS BT 1.00 at certain frequencies (1, 10, 100 kHz). The colossal permittivity of the sintered ceramics decreases in a step-like shape as the temperature decreases, and the relative permittivity becomes independent of temperature below 50 K. This behavior is also found in a well-known high permittivity material CCTO.[8] The decrease of relative permittivity is accompanied by the dielectric loss peak at the given temperature, which indicates a temperature activated dielectric relaxation has occurred: the dielectric loss peaks appear at lower temperatures as frequencies decrease (Figure 3).

Generally, the Debye model can be used to describe the dielectric relaxation, and the relaxation frequency can be represented by

$$\nu = \nu_o \exp\left(-\frac{E_A}{k_B T}\right), \tag{1}$$

where ν_o, k_B, and E_A represent the pre-exponential factor, the Boltzmann constant, and the activation energy for relaxation, respectively.[18] The imaginary part of the dielectric response (ε'') is proportional to $\nu\tau/1+(\nu\tau)^2$, and the maxima of ε'' occurs when $\nu\tau = 1$, where τ is the dielectric relaxation time. Thus, the relaxation temperatures at different frequencies can be extracted from the maximums of ε'' and E_A can be calculated from the Arrhenius plot for Eq. (1).

As such, the ε'' maxima for SPS BT 0.95 and 1.00 are determined from Figure 3 and the Arrhenius plots for the both samples are shown in Figure 4. The change in slope of the fitted curves for SPS BT 0.95 clearly indicates that two different thermally activated polarization mechanisms exist (Figure 4(a)). By contrast, it is hard to distinguish a slope change for SPS BT 1.00 sample (Figure 4(b)). The activation energies of 0.054 eV, 0.078 eV and the jump frequencies of 4.5×10^5 Hz, 1.89×10^6 Hz are obtained for SPS BT 0.95 and 1.00, respectively, in the low temperature region (30 K–100 K), while 0.093 eV, 0.108 eV and 3.57×10^7 Hz, 4.25×10^7 Hz are calculated in the high temperature region (100 K–300 K) (Figure 4). Higher activation energy of the high temperature region is consistent with the co-existence of two polarization mechanisms.

It has been widely investigated that reducing sintering atmosphere (vacuum) of SPS technique can cause high concentration of oxygen vacancies and electrons in the sintered ceramics by[4]

$$O_o^x \rightarrow \frac{1}{2}O_2 + V_o^{\bullet\bullet} + 2e'. \tag{2}$$

Induced oxygen vacancies and electrons can be the localized charge carriers in the grain or at the grain boundary

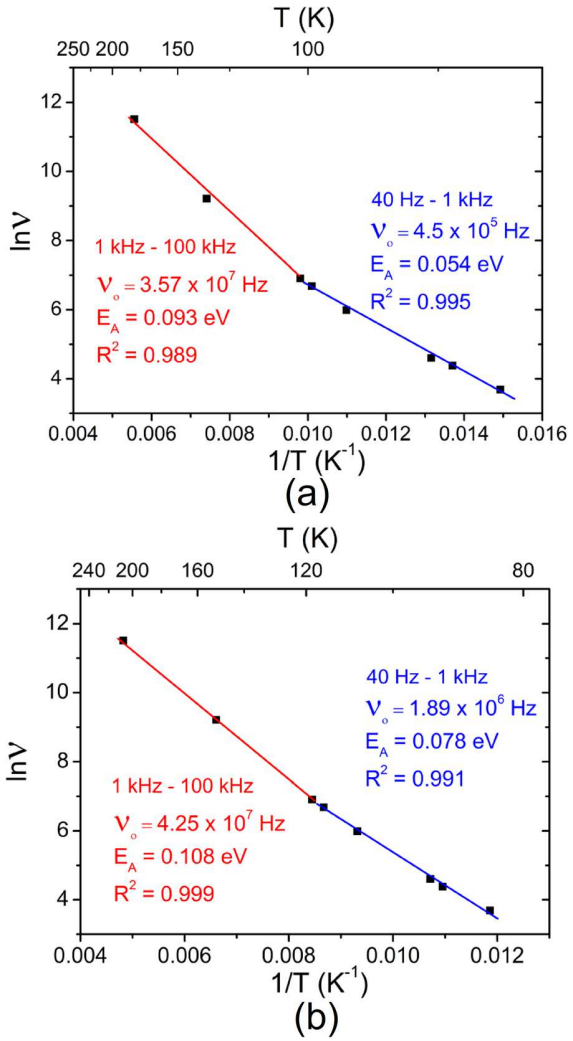

FIG. 4. Activation energy of thermally activated relaxations for (a) SPS BT 0.95 and (b) SPS BT 1.00.

under the applied ac electric field. The origin of colossal permittivity of barium titanate has been widely explained by the interfacial polarization effect by oxygen vacancies in the vicinity of gain boundaries and mobile electrons in the grains.[4,19] However, it is also well known that the localized charge carriers can induce hopping dipoles in the material by polaron hopping such that these can affect dielectric response of the material.[20] Thus, the second polarization mechanism of the colossal permittivity in barium titanate could be attributed to a polaron hopping process in the grains. If that is the case, then the large change of activation energies in SPS BT 0.95 compared to SPS BT 1.00 (Figure 4(a)) could be attributed to the higher concentration of polarons due to non-stoichiometric Ba/Ti ratio of SPS BT 0.95 sample.

To further investigate this hypothesis, the universal dielectric response (UDR) model can be applied in order to link conductivity and dielectric response due to localized charge carriers.[21] According to Jonscher's power law, the relative permittivity can be represented as a power law of ω^{s-1} resulting from the Kramers-Kronig transformation for a power law of the ac conductivity, ω^{s}.[21] Therefore, conductivity (σ') and relative permittivity (ε') can be written as

$$\sigma'(\mathrm{f}) = \sigma_{\mathrm{dc}} + \sigma_{\mathrm{o}}\mathrm{f}^{\mathrm{s}}, \tag{3}$$

$$\varepsilon' = \tan(\mathrm{s}\pi/2)\sigma_{\mathrm{o}}\mathrm{f}^{\mathrm{s}-1}/\varepsilon_{\mathrm{o}}, \tag{4}$$

where σ_{dc} is dc conductivity, σ_o and s represent the temperature dependent constants, and ε_o and f denote the permittivity of free space and experimental frequency ($\mathrm{f} = \omega/2\pi$), respectively. Equation (4) also can be written as

$$\mathrm{f}\varepsilon' = \mathrm{A(T)f}^{\mathrm{s}}, \tag{5}$$

where $A(T) = \tan(s\pi/2)\sigma_o\varepsilon_o$ and s is the constant value between 0 and 1. Thus, a straight line should appear in $\log_{10}(\varepsilon'_{\mathrm{r}}\mathrm{f})$ vs. $\log_{10}(f)$ plot at the given temperature, and the slope of the line indicates the value of s.

Figure 5 represents the $\log_{10}(\varepsilon'_{\mathrm{r}}\mathrm{f})$ vs. $\log_{10}(\mathrm{f})$ plot for SPS BT 0.95 at different temperatures (30 K–300 K). A straight line does appear at high temperatures and low frequencies. However, the straight line is deviated from the slope as frequency increases due to relaxation, and consequently it decreases in a step-like shape and forms another straight line at the high frequency region. As temperature decreases, deviations from the slope are gradually occurred at lower frequencies as relaxation frequencies shift to lower frequencies at lower temperature (Figure 5). The values of s are found to be 0.98 and 0.95 when obtained from the slopes at high and low temperature regions, respectively. It should be noted that the value of s as closer to "1" indicates polarization charges that are more strictly localized.[22]

In the standard polaron model, the value of s tends to increase and becomes closer to "1" as temperature decreases since the hopping dipoles freeze at low temperatures.[22] Interestingly, however, it is shown here that for the colossal permittivity of BT, the value of s decreases as temperature decreases, which means charge carriers for polarization are less localized at low temperatures when compared to high temperatures. This indicates that, while hopping polarization is becoming inactive at low temperatures due to insufficient energy to overcome energy barrier for polarization, interfacial polarization associated with mobile electrons in the grains and oxygen vacancies at the vicinity of the grain boundaries are still active as a polarization mechanism.

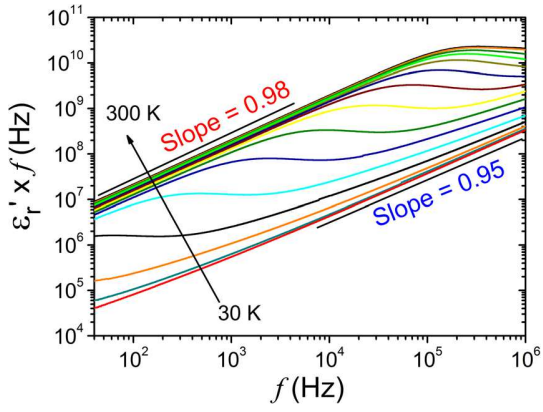

FIG. 5. $\mathrm{Log}_{10}(\varepsilon'_{\mathrm{r}}\mathrm{f})$ vs. $\log_{10}\mathrm{f}$ plot for the SPS (1150 °C) BT at different temperatures (30 K–300 K).

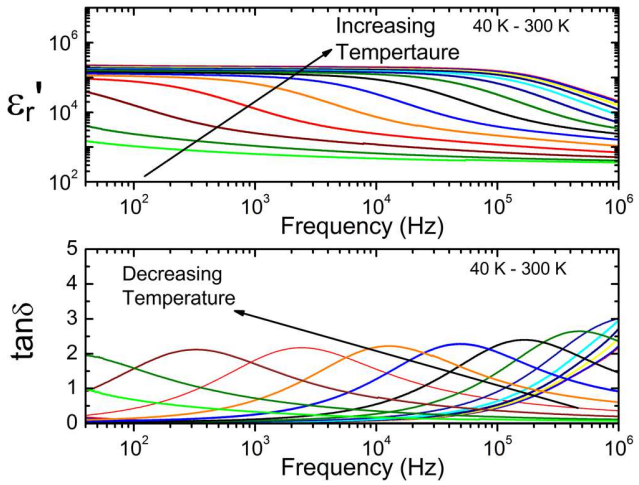

FIG. 6. Dielectric properties of SPS BT 0.95 sample as a function of frequency (40 Hz–1 MHz) at different temperatures (40 K–300 K).

Thus, the lower value of s may be due to the fact that the electrons for interfacial polarization are free to move in the grains compared to hopped electrons with oxygen vacancies for hopping polarization.

Figure 6 shows the permittivity and dielectric loss change of the SPS BT 0.95 sample as a function of frequency (40 Hz–1 MHz) at different temperatures (40 K–300 K). At high temperatures, both polarization mechanisms (space charge and polarons) are able to contribute to the colossal permittivity of BT and form the upper plateau (Figure 6). As frequency increases, the permittivity decreases significantly with a correlated dielectric loss peak (Figure 6). This is consistent with dielectric relaxation as described by Debye theory,[18] where relaxation frequencies are also shifted to lower frequencies as temperature decreases.

To further depict this behavior, the relative permittivity and dielectric loss of SPS BT 0.95 between 40 Hz and 1 MHz are separately shown in Figure 7 for representative temperatures across the range investigated (i.e., 300 K, 160 K, 100 K, and 30 K). It is observed that an extremely high permittivity of up to 2.4×10^5 and dielectric loss below 0.1 are achieved at 300 K between 40 Hz and 10 kHz. This behavior has been previously referred to as colossal permittivity, even though in prior cases the dielectric loss was significantly larger (above 1.0), thus implying conduction processes.[4] Here, the colossal permittivity is maintained ($\varepsilon' > 10^5$) up to 100 kHz, however, it drops significantly as frequency increases from 100 kHz to 1 MHz, and correspondingly dielectric loss shows sharp increases to $\tan\delta \approx 2.8$ (Figure 7(a)); this physically meaningless value is rather a clear indication of the onset of conductivity at those higher frequencies.

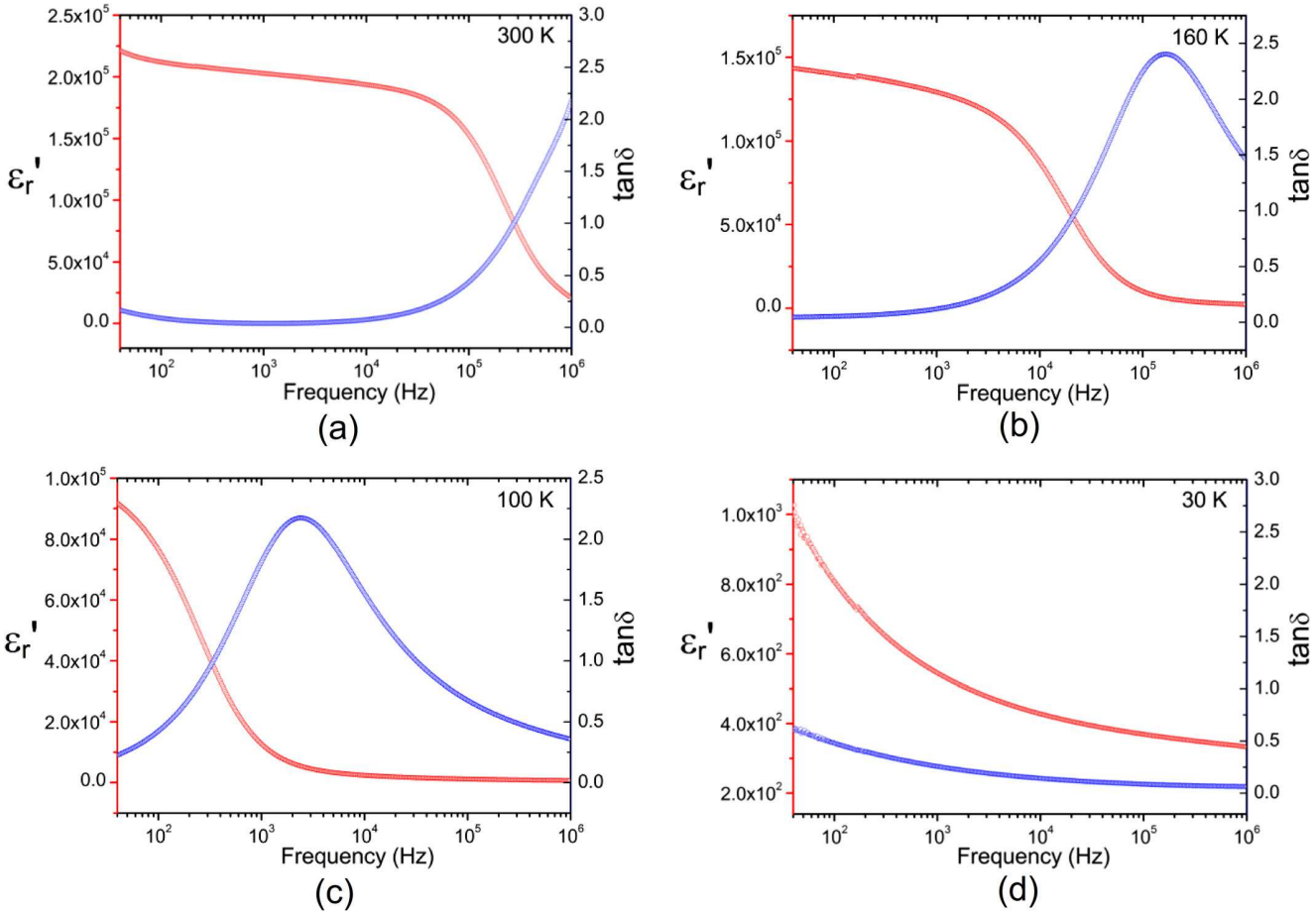

FIG. 7. Dielectric properties of SPS BT 0.95 at 300 K, 160 K, 100 K, and 30 K in the frequency range of 40 Hz–1 MHz.

By contrast, at low temperature, no colossal permittivity is observed and, for example, at 30 K, the highest permittivity is ~1000. Moreover, the decrease in relative permittivity as the measuring frequency increases is markedly different when low and high temperature responses are compared. At high temperature (Figure 7(a)), permittivity, it is clear that the drop in permittivity undergoes two relaxation mechanisms with different characteristic frequencies, while at low temperature, only one relaxation mechanism with very low characteristic frequency is active (Figure 7(d)). This further confirms that interfacial and polaron hopping polarizations contribute to the colossal permittivity at high temperatures (300 K); however, only interfacial (space charge) polarization is active at low temperatures (30 K), which is consistent with the UDR analysis.

Furthermore, to gain insight into the physical characteristics of the processes driving these relaxations, it is important to recall that in the thermally activated polaron hopping model, the maximum of the imaginary part of the relative permittivity, ε'', is related to the number of hopping polarons by

$$\varepsilon''_{max} = N\mu^2/3k_BT, \tag{6}$$

where N and μ represent the number of hopping polarons and the hopping dipole moment, respectively. N is exponentially dependent on the temperature, which can be written as

$$N = N_o \exp(-E_A/k_BT), \tag{7}$$

where N_o is the pre-exponential factor and E_A is the activation energy associated with dielectric relaxation of hopping dipoles.[23,24] Thus, substituting Eq. (7) into Eq. (6) results in

$$T\varepsilon''_{max} = \frac{N_o\mu^2}{3k_B}\exp(-E_A/k_BT). \tag{8}$$

The imaginary part of the relative permittivity for SPS BT 0.95 is plotted in Figure 8 as a function of frequency (40 Hz–1 MHz) between 300 K and 100 K. The ε''_{max} obtained for each temperature was then plotted in the Arrhenius form ($\ln(\varepsilon''_{max}T)$ vs. 1/T) to calculate the activation energy for hopping polarization (Figure 9). It is clear that two linear slopes appear with a transition temperature around 180 K.

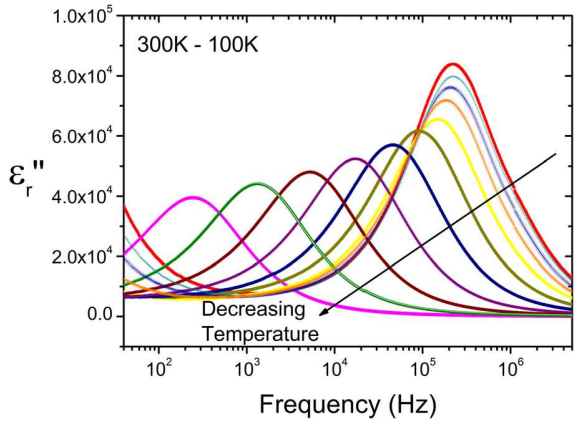

FIG. 8. The imaginary part of the relative permittivity changes for SPS BT 0.95 as a function of frequencies (40 Hz–1 MHz) at 300 K–100 K.

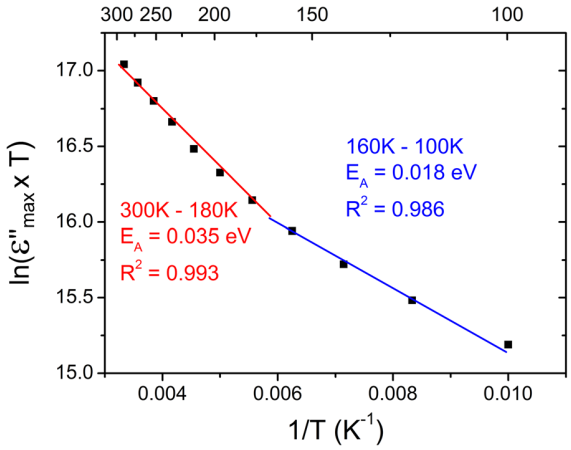

FIG. 9. Activation energy for polaron hopping polarization at 300 K–200 K.

Accordingly, activation energies of 0.035 eV and 0.018 eV are calculated from the fitted line for high (300 K–180 K) and low temperature (160 K–100 K) regions, respectively. Not surprisingly ε''_{max} increases as temperature increases, which further confirms that thermally activated polarization, associated with polaronic dipoles, is a contributing polarization mechanism to the colossal permittivity of BT.

More importantly, comparison between the activation energy for the high temperature (E_{AH}) and low temperature (E_{AL}) regions can reveal the activation energy for the different polarization mechanisms (similar to the analysis of the data in Figure 4) as follows:

$$E_{AH} = E_{AP} + E_{AI}, \tag{9}$$

$$E_{AL} = E_{AI}, \tag{10}$$

where E_{AP} and E_{AI} are the activation energies for hopping polarization and interfacial polarization in the colossal permittivity of BT, respectively. From Figure 4(a), E_{AH} and E_{AL} were calculated as 0.094 eV and 0.054 eV; using these values in Eqs. (9) and (10), E_{AP} of 0.039 eV and E_{AI} of 0.054 eV are obtained. These results are in good agreement with the calculated activation energy ($E_{AP} = 0.035$ eV) for high temperature region by using the thermally activated polaronic model (Figure 9).

Recognizing that various polarization mechanisms are contributing to the observed colossal permittivity, it is important to estimate their relative contribution. To achieve this, the contribution of interfacial polarization to the colossal permittivity at 300 K can be calculated by using the internal barrier layer capacitance (IBLC) model, which can be presented by

$$\varepsilon_{eff} = \frac{\varepsilon_r t_g}{t_b} \tag{11}$$

where ε_{eff}, ε_r, t_g, and t_b are the effective relative permittivity, relative permittivity of the material, grain size, and thickness of grain boundary, respectively. Relative permittivity of barium titanate ($\varepsilon_r \approx 2400$),[25] grain size (56 ± 6 nm, from Figure 1(c)), and thickness of grain boundary (≈1 nm)[26] are used to calculate the effective permittivity of SPS BT 0.95. An

effective permittivity of 1.34×10^5 (equivalent to ~20.12% of the experimentally observed colossal permittivity) is calculated for the SPS BT 0.95 ceramics.

Furthermore, it is well known that noble metal electrodes tend to form Schottky junction with the surfaces of semiconducting BT, and that this can affect dielectric properties of BT at low frequencies.[27] Therefore, here, a variety of electrode materials (i.e., Au, Ag, Ni, and Al) were tested, in order to calculated electrode effect on the colossal permittivity of BT ceramics. It was confirmed that while Au, Ag, and Ni formed a Schottky junction, Al formed ohmic contacts with SPS BT ceramics. Thus, in this way, the electrode effect on the colossal permittivity was estimated by subtracting permittivity measured with Al electrode (not shown here) from measured permittivity with Au. The calculation showed that about 15% of the colossal permittivity of SPS BT ceramics at low frequencies can be attributed to the extrinsic electrode effect. Moreover, the contribution of hopping polarization can also be obtained simply by subtracting the interfacial contribution from the total intrinsic permittivity resulting in 4.34×10^5 (~64.88%). This result is quite comparable with the values which can be extracted from Figure 7(a): $\varepsilon'_{interfacial} \approx 2.9 \times 10^4$ (12.13%) and $\varepsilon'_{polaron} \approx 1.74 \times 10^5$ (73.00%).

It is interesting to note that the low loss ($\tan\delta \approx 0.05$) of SPS BT samples can be attributed to a thin re-oxidation layer on the surfaces associated with the short annealing treatment (850 °C for 15 min). This is further confirmed as the measured dielectric loss of the samples is extensively increased ($\tan\delta > 1.00$) after polishing the surfaces. The surface of the samples becomes insulating after the short annealing process, while the interior is still reduced (semi-conductive). This configuration is comparable with a barrier layer capacitance (BLC) effect and is able to effectively lower the dielectric loss while maintaining the high permittivity of sintered ceramics.[28]

In conclusion, it can be stated that the origin of colossal permittivity in BT ceramics is due to the combination effects of BLC (thanks to an insulating surface), interfacial polarization at the interior insulating grain boundaries, and hopping polarizations in semiconducting grains by a large number of induced charge carriers. These different contributions to the observed colossal permittivity are schematically depicted in Figure 10.

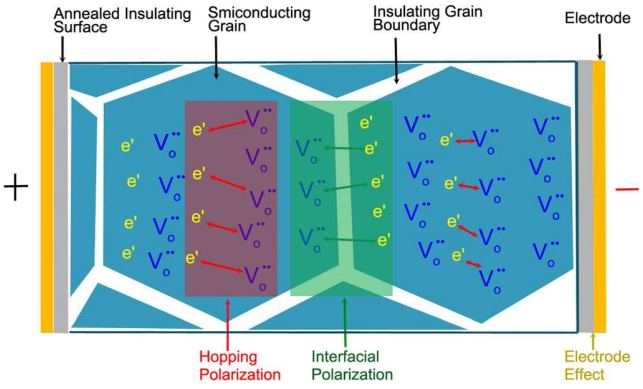

FIG. 10. Interfacial and hopping polarization model for the colossal permittivity of BT ceramics.

IV. CONCLUSION

In the current work, barium titanate ceramics with different Ba/Ti ratios (0.95 and 1.00) were synthesized by spark plasma sintering technique. Scanning electron microscopy revealed that sintered ceramics have nanoscale grains. X-ray diffraction measurements showed additional phases of $BaTi_2O_5$ and $Ba_4Ti_{12}O_{27}$ for the starting powder and sintered ceramic with Ba/Ti ratio of 0.95, respectively. However, no secondary phase was observed for the starting powder and sintered ceramic with Ba/Ti ratio of 1.00. Dielectric measurements demonstrated that sintered ceramics have colossal permittivity up to $\sim 10^5$ at room temperature and 1 kHz. This colossal permittivity can be maintained up to 100 kHz at room temperature. Onset of dielectric relaxation following Debye theory occurred as temperature decreased. Activation energy changes for relaxation indicate that at least two different relaxational polarization mechanisms may be contributing the colossal permittivity in barium titanate. According to UDR model, in addition to interfacial polarization at insulating grain boundary, polarization due to polaron hopping was proposed as a co-existing polarization mechanism in the colossal permittivity of barium titanate ceramics. To this end, relative contributions of each polarization to the colossal permittivity were calculated: ~65% hopping polarization, ~20% interfacial polarization, and ~15% electrode effect.

ACKNOWLEDGMENTS

This work was supported partially by the U.S. National Science Foundation under grant DMR 0449710. The authors thank the DGAC for financial support (ISS2 project).

[1]S. Roberts, Phys. Rev. **71**, 890 (1947).
[2]K. Kinoshita and A. Yamaji, J. Appl. Phys. **47**, 371 (1976).
[3]A. S. Shaikh, R. W. Vest, and G. M. Vest, IEEE Trans. Ultrason. Ferroelectr. Freq. Control **36**, 407 (1989).
[4]S. Guillemet-Fritsch, Z. Valdez-Nava, C. Tenailleau, T. Lebey, B. Durand, and J. Y. Chane-Ching, Adv. Mater. **20**, 551 (2008).
[5]T. Takeuchi, C. Capiglia, N. Balakrishnan, Y. Takeda, and H. Kageyama, J. Mater. Res. **17**, 575 (2002).
[6]M. T. Buscaglia, V. Buscaglia, M. Viviani, J. Petzelt, M. Savinov, L. Mitoseriu, A. Testino, P. Nanni, C. Harnagea, Z. Zhao, and M. Nygren, Nanotechnology **15**, 1113 (2004).
[7]B. R. Li, X. H. Wang, M. M. Cai, L. F. Hao, and L. T. Li, Mater. Chem. Phys. **82**, 173 (2003).
[8]M. A. Subramanian, D. Li, N. Duan, B. A. Reisner, and A. W. Sleight, J. Solid State Chem. **151**, 323 (2000).
[9]C. Pecharroman, F. Esteban-Betegon, J. F. Bartolome, S. Lopez-Esteban, and J. S. Moya, Adv. Mater. **13**, 1541 (2001).
[10]Y. J. Wu, S. H. Su, J. P. Cheng, and X. M. Chen, J. Am. Ceram. Soc. **94**, 663 (2011).
[11]D. C. Sinclair, T. B. Adams, F. D. Morrison, and A. R. West, Appl. Phys. Lett. **80**, 2153 (2002).
[12]T. B. Adams, D. C. Sinclair, and A. R. West, Adv. Mater. **14**, 1321 (2002).
[13]M. Li, A. Feteira, and D. C. Sinclair, J. Appl. Phys. **98**, 084101 (2005).
[14]Z. Valdez-Nava, S. Guillemet-Fritsch, C. Tenailleau, T. Lebey, B. Durand, and J. Y. Chane-Ching, J. Electroceram. **22**, 238 (2009).
[15]H. Abrams, Metallography **4**, 59 (1971).
[16]S. Lee, C. A. Randall, and Z. K. Liu, J. Am. Ceram. Soc. **91**, 1753 (2008).
[17]T. Takeuchi, M. Tabuchi, H. Kageyama, and Y. Suyama, J. Am. Ceram. Soc. **82**, 939 (1999).
[18]J. R. Macdonald, *Impedance Spectroscopy* (Wiley, New York,1987).
[19]M. Maglione, *Solid-State Science*, Springer Series of Topics, edited by V. S. Vikhnin and G. K. Liu, (Springer, New York, 2008).

[20]Y. H. Li, L. Fang, L. J. Liu, Y. M. Huang, and C. Z. Hu, Mater. Sci. Eng. B **177**, 673 (2012).
[21]A. K. Jonscher, J. Phys. D: Appl. Phys. **32**, R57 (1999).
[22]A. S. Nowick and B. S. Lim, Phys. Rev. B **63**, 184115 (2001).
[23]L. L. Hench and J. K. West, *Principles of Electronic Ceramics* (John Wiley & Sons, New York, 1990).
[24]S. Komine and E. Iguchi, J. Phys.: Condens. Matter **16**, 1061 (2004).
[25]G. Arlt, D. Hennings, and G. Dewith, J. Appl. Phys. **58**, 1619 (1985).
[26]Z. Valdez-Nava, C. Tenailleau, S. Guillemet-Fritsch, N. El Horr, T. Lebey, P. Dufour, B. Durand, and J. Y. Chane-Ching, J. Phys. Chem. Solids **72**, 17 (2011).
[27]W. Heywang, J. Mater. Sci. **6**, 1214 (1971).
[28]A. J. Moulson and J. M. Herbert, *Electroceramics* (Champman and Hall, London, 1990).